





## Research Article

# Mechanism and Characteristics of CH<sub>4</sub>/CO<sub>2</sub>/H<sub>2</sub>O Adsorption in Lignite Molecules

Zhihui Wen <sup>1,2,3</sup> Yunpeng Yang <sup>1,2</sup> Qi Wang <sup>1,2</sup> and Banghua Yao <sup>1,2,3</sup>

<sup>1</sup>School of Safety Science and Engineering, Henan Polytechnic University, Jiaozuo 454000, China

<sup>2</sup>State Key Laboratory Cultivation Base for Gas Geology and Gas Control (Henan Polytechnic University), Jiaozuo 454000, China

<sup>3</sup>State Collaborative Innovation Center of Coal Work Safety and Clean-Efficiency Utilization, Jiaozuo 454000, China

Correspondence should be addressed to Zhihui Wen; wenzhihui@hpu.edu.cn

Received 21 January 2021; Revised 19 February 2021; Accepted 9 March 2021; Published 20 March 2021

Academic Editor: Yi Xue

Copyright © 2021 Zhihui Wen et al. This is an open access article distributed under the Creative Commons Attribution License, which permits unrestricted use, distribution, and reproduction in any medium, provided the original work is properly cited.

Adsorption characteristics of coalbed methane (CBM) are significant to investigate the absorption of coal, shale, and porous media. In particular, adsorption characteristics of CH<sub>4</sub>, CO<sub>2</sub>, and H<sub>2</sub>O play an important role in predicting CBM output and geologic sequestration potentials of CO<sub>2</sub> in research fields of CO<sub>2</sub>-enhanced CBM recovery (CO<sub>2</sub>-ECBM) and sequestration of CO<sub>2</sub>. In this work, adsorption characteristics of CH<sub>4</sub>, CO<sub>2</sub>, and H<sub>2</sub>O in lignite molecules were simulated through the grand canonical Monte Carlo (GCMC) method and molecular dynamics (MD) method. Research results demonstrated that given the same temperature and pressure, the ultimate adsorption capacity of lignite per unit to H<sub>2</sub>O is the highest, followed by those of CO<sub>2</sub> and CH<sub>4</sub> successively. All isothermal adsorption curves conform to the “I-type” characteristics. In the saturated molecular configuration, gas molecules show different distribution patterns at two sides of the lignite molecule chain. Lignite has typical physical adsorption to CH<sub>4</sub> and CO<sub>2</sub>, with adsorption energy provided by nonbonding energy. However, lignite has both physical adsorption and chemical adsorption to H<sub>2</sub>O, with adsorption energy provided by both nonbonding energy and hydrogen bond energy. High temperature is against adsorption of CH<sub>4</sub>, CO<sub>2</sub>, and H<sub>2</sub>O. Temperature might inhibit adsorption of gas molecules. Research conclusions lay foundations for the exploitation and development of CBM and relevant studies on sequestration of CO<sub>2</sub>.

## 1. Introduction

Recently, the energy problem has become an important global research field. With the increasing exhaustion of fossil fuels, it is crucial to find new energies [1, 2]. Coalbed methane (CBM), a high-efficiency, environmental-friendly, and rich energy source, has been highly concerned by scholars and experts [3–7]. It is the best substitute for fossil fuels at present. CBM is mainly composed of CH<sub>4</sub>, CO<sub>2</sub>, H<sub>2</sub>O, O<sub>2</sub>, and some other trace gases, and 80%–90% of CBM are adsorbed on the surface of the coal matrix [8, 9]. According to estimations, the global CBM resources are higher than 200,000 billion m<sup>3</sup>. China also possesses abundant CBM reserves, and it is the third-largest CBM reserve in the world. There are about 35,000 billion m<sup>3</sup> of CBM resources in more than 2,000 m of buried depth, including about 12,000 m<sup>3</sup> of explored reserves and 23,000 m<sup>3</sup> of future reserves. There is

a great development potential of CBM resources in China [10, 11]. Meanwhile, exploiting CBM before coal mining can avoid the occurrence of outburst of gas and gas explosion effectively. Injecting CO<sub>2</sub> to enhance coalbed methane (CO<sub>2</sub>-ECBM) has been widely concerned by many scholars because it can not only displace the methane in coal but also reduce the greenhouse gas effect by geological storage [12, 13]. Many studies have demonstrated that the total pore volume of coals is mainly determined by micropores (<2 nm) and mesopores (2–50 nm) [14–16]. Therefore, elaborating the microscale adsorption characteristics and mechanism of coals is critical to adopt effective CO<sub>2</sub>-ECBM measures and gas disaster control technologies. Therefore, it is very necessary to carry out molecular simulation on adsorption of CH<sub>4</sub>, CO<sub>2</sub>, and H<sub>2</sub>O in coal matrix molecules.

With the development of scientific technology, the molecular adsorption mechanism between adsorbent and

adsorbate can be discussed through computer molecular simulation. Microscopic technology is very suitable to study adsorption behavior of nanometer and submicron pores of coals [17]. Matranga et al. [18] simulated the adsorption behavior of  $\text{CH}_4$ ,  $\text{CO}_2$ , and  $\text{N}_2$  on activated carbons by the grand canonical Monte Carlo (GCMC) method, finding that the adsorption capacity and adsorption heats of  $\text{CO}_2$  are higher than those of  $\text{CH}_4$  and  $\text{N}_2$ . Narkiewicz and Mathews [19] introduced an adsorption position corresponding to the  $\text{CO}_2$  adsorption of low-volatile soft coals and methane molecular capacity and model through molecular simulation. Zhang et al. [20] discussed adsorption effects of benzene ring and side chains of coal surface molecules to  $\text{CH}_4$ ,  $\text{CO}_2$ ,  $\text{N}_2$ , and  $\text{O}_2$  through molecular simulation. Xiang et al. [21] concluded adsorption capacities of  $\text{CH}_4$ ,  $\text{CO}_2$ , and  $\text{H}_2\text{O}$ , molecular configuration, and effects of oxygen-containing functional groups on adsorption performance of Yanzhou coal through GCMC and MD methods. Mosher et al. [14] carried out a molecular simulation to explore competitive adsorption behaviors of  $\text{CH}_4$  and  $\text{CO}_2$  in micropores and middle pore structures of coals. Dang et al. [22] and Song et al. [23] studied adsorption behaviors of  $\text{CH}_4$ ,  $\text{CO}_2$ , and  $\text{H}_2\text{O}$  in low-rank coals by using density functional theory (DFT) and MD, finding that high temperature is against adsorption of  $\text{CH}_4$ ,  $\text{CO}_2$ , and  $\text{H}_2\text{O}$  in coal matrix and oxygen-functional groups and nitrogen-containing functional groups of coal can influence adsorption greatly. Xu et al. [24] studied molecular behaviors that  $\text{CO}_2$  promotes  $\text{CH}_4$  desorption in coals. You et al. [25] simulated the interaction between subbituminous coals and water through MD simulation and found that water molecules are easy to be adsorbed by carboxyls. Li et al. [26] calculated and discussed adsorption capacities of  $\text{CH}_4$ ,  $\text{CO}_2$ , and  $\text{N}_2$  in coal silt models, finding a relationship in adsorption capacities of three gases with the increase of silt width:  $\text{H}_2\text{O} > \text{CH}_4 > \text{N}_2$ . Gao et al. [27] simulated adsorption characteristics of lignite through GCMC and MD methods. Results showed that the adsorption isotherm of single gas conformed to the Langmuir equation and the  $\text{CO}_2$  enjoys obvious advantages in the competitive adsorption of multiple gases. Hu et al. [28] and You et al. [29] studied self-diffusion and mutual diffusion of  $\text{CH}_4$ ,  $\text{CO}_2$ , and multicomponent gases through the MD method.

Although many works have been reported, only few concentrate on adsorption characteristics of  $\text{CH}_4$ ,  $\text{CO}_2$ , and  $\text{H}_2\text{O}$  in lignite. Besides, lignite reserves account for 47% of total coal reserves, indicating that lignite has great potentials in CBM development and sequestration of  $\text{CO}_2$ . In this study, adsorption characteristics of  $\text{CH}_4$ ,  $\text{CO}_2$ , and  $\text{H}_2\text{O}$  in lignite which possesses a great reserve were discussed with the classical GCMC and MD method. Moreover, the stable configuration of lignite molecules was discussed, and the saturated adsorption capacity and saturated molecular configuration of lignite molecules were simulated. The variation law of adsorption energy of different adsorbates in lignite molecules was analyzed, and the microscopic mechanism of  $\text{CH}_4$ ,  $\text{CO}_2$ , and  $\text{H}_2\text{O}$  adsorption in lignite molecules was elaborated. Research conclusions provide theoretical supports to study adsorption performances of different adsorbates in lignite molecules.

## 2. Methodology

**2.1. Brown Coal Structure Construction.** Coal is a type of porous heterogeneous solids with complicated physical and chemical structures. The basic structural unit of coals includes a regular part and irregular part. The regular part is composed of benzene rings, heterocyclic rings, alicyclic rings, and hydroaromatic rings, and it forms the core part of the structural unit of coals. The irregular part is composed of functional groups which are connected to the regular part and side chains of alkyls. Among studies of the molecular structure of coals, more than 130 molecular structures have been proposed yet [30]. Among them, the Given model [31], Wisser model [32], and Solomon model [33] are representative ones. In particular, the Wisser model is regarded as a relatively comprehensive and reasonable model to describe lignite with a low degree of metamorphism, and this model can reflect the modern concept of the molecular structure of coals. The Wisser model can explain surface chemical and other reactive properties of lignite. Therefore, it is widely applied in simulation studies related to lignite molecules [17, 26, 33]. The Wisser model ( $\text{C}_{184}\text{H}_{155}\text{N}_3\text{O}_{20}\text{S}_3$ ) has basic features of lignite, including a single aromatic ring which is linked and cross-linked through the aliphatic side chain. It is applicable to the molecular simulation study of gas adsorption of lignite. The plane molecular structure of the Wisser model is shown in Figure 1.

In this work, Materials Studio (MS) was used to carry out the simulation calculation. In the MS, 3D lignite molecular structural units were constructed according to the molecular formula ( $\text{C}_{184}\text{H}_{155}\text{N}_3\text{O}_{20}\text{S}_3$ ), and they were defined as a molecular fragment. The initial 3D space structure of lignite molecules was gained by adding hydrogen until saturation. In the Condensed-phase Optimized Molecular Potentials for Atomistic Simulation Studies (COMPASS), the smart technique was chosen to optimize the initial 3D spatial structure of lignite molecules. The number of iteration steps, convergent standard accuracy, and energy deviation were set as 100,000, fine, and 0.0001 kcal/mol, respectively. The acting energies of Coulomb electrostatic force and Van der Waals (VDW) force were set at the atomic state, and charges carried on the lignite molecular structure were distributed automatically by a force field. Potential energy surfaces were searched through annealing added with energy disturbance to recognize the point with the lowest energy in the system. The frame with the lowest energy was chosen as the stable structure of the molecular structural model of lignite. The optimized 3D structure of lignite molecules is shown in Figure 2.

In order to verify the accuracy of the constructed molecular model of lignite, unit cells were added through setting of density to the stable molecular model of lignite in Figure 2 by using the Amorphous Cell module. The constructed unit cells were processed by MD optimization and annealing, thus getting stable configuration and energy distribution of unit cells under different densities. The molecular structure at the lowest system energy is the most stable. At this moment, the density corresponding to the system energy is the optimal density after adding periodic boundary conditions. The

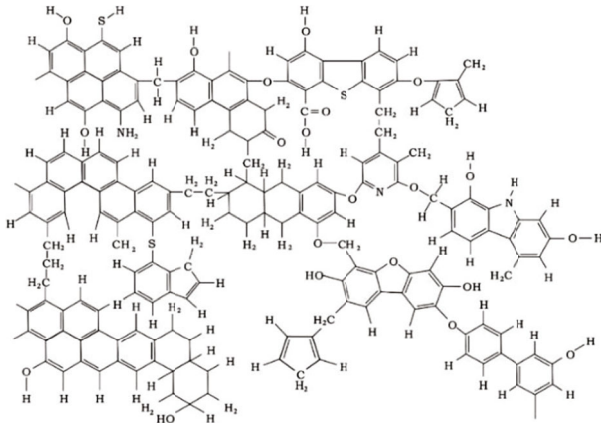


FIGURE 1: Molecular plane structure of the Wisser model [28].

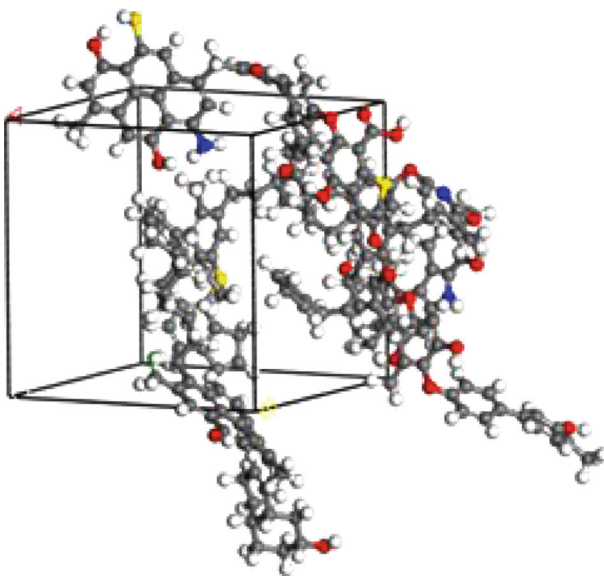


FIGURE 2: Stable molecular model of lignite. Color scheme: C: black; H: gray; O: red; N: blue; S: yellow.

variation laws of unit cell system energy of lignite with density are shown in Figure 3.

It can be seen from Figure 3(b) that with the increase in system density, system energy of lignite molecules presents a “V-shaped” variation after unit cells are added in. The system energy of unit cells of lignite fluctuates when the molecular density is between  $1.20 \text{ g/cm}^3$  and  $1.26 \text{ g/cm}^3$  (Figure 3(a)). When the molecular system density of lignite is  $1.23 \text{ g/cm}^3$ , the system energy of unit cells reaches the minimum. Besides, the system energy of unit cells shows an upward trend with the increase and decrease of system density. In other words, the system energy of unit cells of lignite reaches the lowest when the system density is  $1.23 \text{ g/cm}^3$ . Under this circumstance, the molecular structure of lignite is the most stable and the molecular configuration of lignite is the optimal one when periodic boundary conditions are added in. This conforms to the mean lignite density ( $1.21 \text{ g/cm}^3$ ) which is calculated in References [34, 35]. Therefore, the constructed model can be used to investigate the adsorption characteristics in lignite molecules. At this

moment, the unit cell size of lignite molecules is  $1.5745695 \text{ nm} \times 1.5745695 \text{ nm} \times 1.5745695 \text{ nm}$ .

**2.2. Force Field.** In molecular simulation calculations, various types of force fields are used, including (a) the classic fields, such as the MM force field, AMBER force field, CHARMM force field, and CVFF force field, and (b) the second generation fields, such as the COMPASS force field. The existing force field has been highly applicable to description of macromolecular substances and biomacromolecules [26, 36–38]. The molecular force field is formed by a set of potential functions and dynamic constant. The total molecular energy is the sum of kinetic energies and potential energies. Potential energy of molecules can be expressed in a simple geometric coordinate function.

The force field used in this study is a second-generation field. The force field is designed to accurately calculate various properties, structures, spectra, thermodynamic properties, and other expected parameters of a molecule. Thus, in addition to incorporating an enormous amount of experimental data, the derivation of the force-field constant refers to the exact quantum calculation results. Due to the use of varying parameters, second-generation force fields can be divided into various types: CFF91, CFF95, PCFF, and MMFF93.

An appropriate force field should be able to reproduce experimental results quantitatively. We have used different force fields, such as polymer-consistent force field (PCFF), Dreiding, condensed phase optimized molecular potential for atomistic simulation studies (COMPASS), and universal force field, to calculate the density of the lignite molecule model. The results indicated that the density computed through Dreiding force field was the closest to the experimental values. The PCFF force field selected for this study was derived from the CFF91 force field, which is suitable for the study of polymers and organic matter. In addition to the parameters of the force field of CFF91, PCFF contains the force-field parameters of inert gas atoms, such as He, Kr, and metal atoms. These parameters could be used to reckon the molecular system containing these atoms.

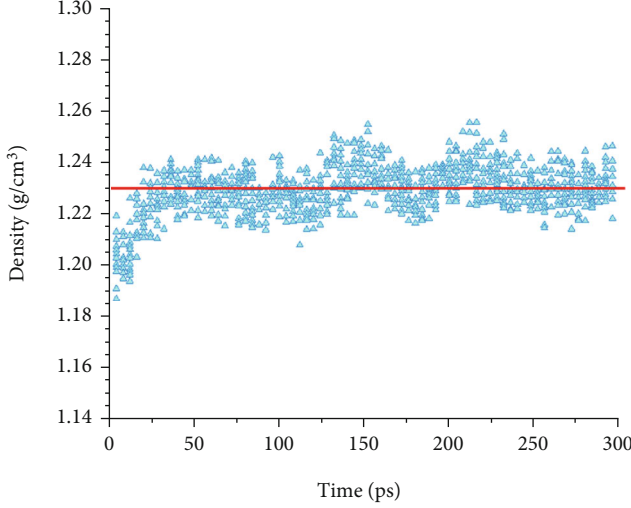
The total energy of a molecule was considered to be the sum of the kinetic and potential energies. The bonding energy includes energy of slip keys ( $E_b$ ), bending energy of bond angle ( $E_\theta$ ), torsion energy of the bond dihedron ( $E_\varphi$ ), bending energy of bond angle surface ( $E_\chi$ ), and crossing energy ( $E_{\text{cross}}$ ). The nonbonding energy covers Coulomb electrostatic force ( $E_c$ ) and VDW force ( $E_v$ ). The total energy of the molecular simulation system ( $E_{\text{total}}$ ) can be expressed as

$$E_{\text{total}} = E_b + E_\theta + E_\varphi + E_\chi + E_{\text{cross}} + E_v + E_c. \quad (1)$$

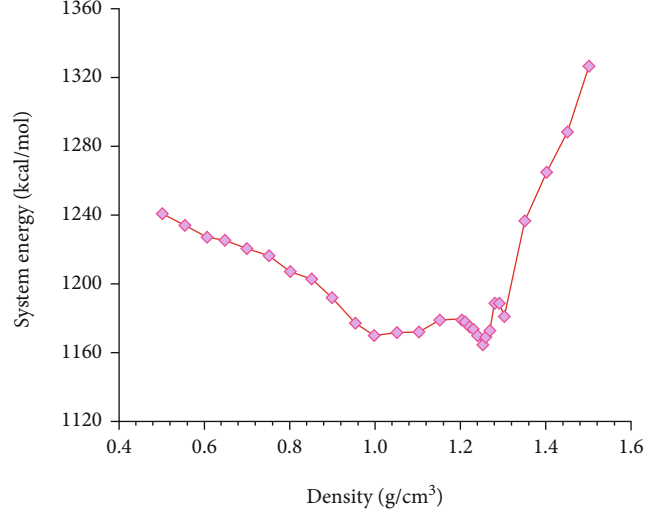
$E_b$  of atoms can be expressed as

$$E_b = \sum_b [K_2(b - b_0)^2 + K_3(b - b_0)^3 + K_4(b - b_0)^4], \quad (2)$$

where  $K_2$ ,  $K_3$ , and  $K_4$  are the elastic constant of chemical bonds, respectively.  $b$  and  $b_0$  are the chemical bond length



(a) Density change during annealing kinetics



(b) System energy change with density

FIGURE 3: Variation of energy with density in unit cell system of lignite.

and bond length at the equilibrium state, respectively. With the decrease of the elastic constant, the vibrational frequency and vibration amplitude slow down and decrease, respectively.  $E_\theta$  can be expressed as

$$E_\theta = \sum_{\theta} [H_2(\theta - \theta_0)^2 + H_3(\theta - \theta_0)^3 + H_4(\theta - \theta_0)^4], \quad (3)$$

where  $\theta$  and  $\theta_0$  are the bond angle and bond angle at the equilibrium state, respectively.  $H_2$ ,  $H_3$ , and  $H_4$  are the bending elastic constants of the bond angle, respectively.  $E_\varphi$  can be expressed as

$$E_\varphi = \sum_{\varphi} \{V_1 [1 - \cos(\varphi - \varphi_1^0)] + V_2 [1 - \cos(2\varphi - \varphi_2^0)] + V_3 [1 - \cos(3\varphi - \varphi_3^0)]\}, \quad (4)$$

where  $V_2$ ,  $V_3$ , and  $V_4$  are the torsion elastic constant of the dihedral angle.  $\varphi$  refers to four adjacent dihedral angles which are not formed by atoms on the same plane.  $\varphi_0$  can be used to reflect the dihedral angle in the initial stage.  $E_\chi$  can be expressed as

$$E_\chi = \sum_{\chi} K_\chi \chi^2, \quad (5)$$

where  $K_\chi$  is the bending elastic constant of the bond angle out of the plane.  $\chi$  denotes the bending angle out of the plane.  $E_{\text{cross}}$  of bonds, bond angles, and dihedral angles can be expressed as

$$\begin{aligned} E_{\text{cross}} = & \sum_b \sum_{b'} F_{bb'} (b - b_0) (b' - b'_0) + \sum_{\theta} \sum_{\theta'} F_{\theta\theta'} (\theta - \theta_0) \\ & \cdot (\theta' - \theta'_0) + \sum_b \sum_{\theta} F_{b\theta} (b - b_0) (\theta - \theta_0) \\ & + \sum_b \sum_{\varphi} (b - b_0) [V_1 \cos \varphi + V_2 \cos 2\varphi + V_3 \cos 3\varphi] \\ & + \sum_{b'} \sum_{\varphi} (b' - b'_0) [V_1 \cos \varphi + V_2 \cos 2\varphi + V_3 \cos 3\varphi] \\ & + \sum_{\theta} \sum_{\varphi} (\theta - \theta_0) [V_1 \cos \varphi + V_2 \cos 2\varphi + V_3 \cos 3\varphi] \\ & + \sum_{\varphi} \sum_{\theta} \sum_{\theta'} K_{\theta\varphi\varphi'} \cos \varphi (\theta - \theta_0) (\theta' - \theta'_0), \end{aligned} \quad (6)$$

where  $F_{bb'}$  is an extended coupling elastic constant,  $F_{\theta\theta'}$  denotes the bending coupling elastic constant,  $F_{b\theta}$  refers to the coupling elastic constant of extended bending, and  $K_{\theta\varphi\varphi'}$  refers to the coupling elastic constant of torsional bending.  $E_c$  can be expressed as

$$E_c = \sum_{ij} \frac{q_i q_j}{r_{ij}}, \quad (7)$$

where  $q_i$  and  $q_j$  are the quantity of electric charge of atoms.  $r_{ij}$  refers to the distance between two atoms. The nonbonded VDW forces ( $E_v$ ) can be expressed as

$$E_v = 4\epsilon_{ij} \left[ \left( \frac{\sigma_{ij}}{r_{ij}} \right)^{12} - \left( \frac{\sigma_{ij}}{r_{ij}} \right)^6 \right], \quad (8)$$

where  $\epsilon_{ij}$  is the effective dielectric constant between two atoms and  $\sigma_{ij}$  is the potential parameter which changes according to the atom type.

### 2.3. Implementation of Simulation

**2.3.1. Optimization of Adsorbate.** Molecular structures of adsorbates CH<sub>4</sub>, CO<sub>2</sub>, and H<sub>2</sub>O are plotted by Skirt in MS, and a 3D atom document of gas molecules is constructed. The plotted molecular structures of adsorbates were cleaned, followed by optimization of molecular mechanical structures and annealing processing under the Focite module. In this process, parameters were set consistent with those in Section 2 for molecular optimization of coals.

**2.3.2. Simulation Scheme and Parameter Setting.** This study is a GCMC simulation based on the Sorption module in MS software. During simulation, the number of gas molecules is added to the coal surface one by one. The coal surface will release heats after adsorption with gas molecules, leading to the energy of the system declining gradually. The system energy reaches the minimum at saturated adsorption of gas molecules in coal structures. Under this circumstance, the number of gas molecules adsorbed on the coal surface is the maximum adsorption capacity of the coal surface to the gas molecule.

During GCMC simulation of adsorption behaviors based on the Sorption module, the task term chose “adsorption isotherm,” and the interaction force between lignite molecules and gas molecules chose “Ewald” and “atom-based.” The electrostatic force was calculated by Ewald, and the VDW force was calculated by the atom-based method. The interaction between lignite molecules and gas molecules was described by the Lennard-Jones (LJ) 12-6 electric potentials [39]. Meanwhile, classical Metropolis rules were used to accept or reject production, disappear, translation, and rotation of gas micromolecules to assure that the system is at the lowest energy state [40]. The temperature in simulation was cycled five times automatically. Step length was adjusted and calculated automatically. The whole simulation involved  $2 \times 10^7$  Monte Carlo steps. The first  $10^7$  steps were set to reach the adsorption equilibrium of the system, while the rest  $10^7$  steps were for sampling and statistics of relevant thermodynamic parameters.

This work is to construct an optimized stable configuration of lignite for adsorbent, and the adsorbates are CH<sub>4</sub>, CO<sub>2</sub>, and H<sub>2</sub>O molecules. The simulation adopted 0.00 MPa~10.00 MPa pressure and periodic boundary conditions. Two situations were involved in the simulation:

- (1) The adsorption characteristics of CH<sub>4</sub>, CO<sub>2</sub>, and H<sub>2</sub>O in lignite molecules under the temperature of 303.15 K were simulated. The saturated adsorption configuration was analyzed, and the evolution laws of energies in the adsorption process were discussed
- (2) Effects of simulation temperatures (283.15 K, 303.15 K, and 323.15 K) on CH<sub>4</sub>, CO<sub>2</sub>, and H<sub>2</sub>O in lignite were analyzed

The adsorption capacity gained in the simulation refers to the number of gas molecules adsorbed in a single unit cell. Its unit is molecular/u.c., but the unit of adsorption capacity in a conventional experiment is cm<sup>3</sup>/g. These adsorption

capacities in different units can be converted according to the following formula:

$$1 \text{ molecular/u.c.} = 1/N \times 10^3 \div M = 1/N \div M \times V_{\text{mol}}, \quad (9)$$

where  $N$  is the Avogadro's constant which values  $6.02 \times 10^{23}$ .  $M$  refers to the mass of a single unit cell, and it is  $4.08017 \times 10^{-21}$  g.  $V_{\text{mol}}$  refers to the molar volume of gas under standard conditions, and it is  $22.4 \times 10^3$  cm<sup>3</sup>/mol.

## 3. Results and Discussion

**3.1. Adsorption Isotherms and Adsorption Capacity.** The adsorption performance of coal is usually expressed by the adsorption isotherm of coal. The adsorption isotherm refers to the curve of the change of coal's adsorption gas volume with gas pressure at a certain fixed temperature. A large number of research results at home and abroad show that when coal adsorbs gas, the adsorption isotherm conforms to the Langmuir adsorption equation expressed as

$$V = \frac{abp}{1 + bp}, \quad (10)$$

where  $V$  is adsorption capacity (cm<sup>3</sup>/g),  $a$  is Langmuir adsorption constant (cm<sup>3</sup>/g),  $b$  is Langmuir adsorption constant (1/MPa), and  $p$  is gas pressure (MPa).

Firstly, GCMC molecular simulation on adsorption isotherm of single pure CH<sub>4</sub>, CO<sub>2</sub>, or H<sub>2</sub>O was carried out under 303.15 K and 0.00 MPa~10.00 MPa. Results are shown in Figure 4.

Evident differences in adsorption capacities of CH<sub>4</sub>, CO<sub>2</sub>, and H<sub>2</sub>O in lignite are observed in Figure 4. In particular, with the increase in adsorption pressure, the adsorption capacity soars up in the low-pressure stage. However, such growth rate declines significantly when the adsorption pressure reaches a fixed value. This indicates that the pressure can promote adsorption behavior. In view of the upward trend of adsorption capacity of lignite per unit mass, the H<sub>2</sub>O adsorption in lignite is significantly faster than those of CO<sub>2</sub> and CH<sub>4</sub> in the low-pressure stage. The CO<sub>2</sub> adsorption in lignite is the second fast, and the CH<sub>4</sub> adsorption is the slowest. In the high-pressure stage, the adsorption rates of CH<sub>4</sub>, CO<sub>2</sub>, and H<sub>2</sub>O in lignite tend to be stable. The simulation results could describe adsorption characteristics of CH<sub>4</sub>, CO<sub>2</sub>, and H<sub>2</sub>O on the lignite surface well by using the Langmuir equation. The gained isothermal curves show good “I-type” characteristics [41], which conform to previous research results [21, 22, 42]. It can be seen from Figure 4 that given the same temperature and pressure, the ultimate adsorption capacities of CH<sub>4</sub>, CO<sub>2</sub>, and H<sub>2</sub>O in lignite per unit mass observe the laws of H<sub>2</sub>O > CO<sub>2</sub> > CH<sub>4</sub>. This was consistent with previous research results based on simulation [16, 17, 21, 26].

**3.2. Adsorption Saturation Configuration.** The saturated molecular configuration of lignite molecules cannot be displayed clearly due to the influences of a single unit cell. The molecular configuration of the unit cell was extended for

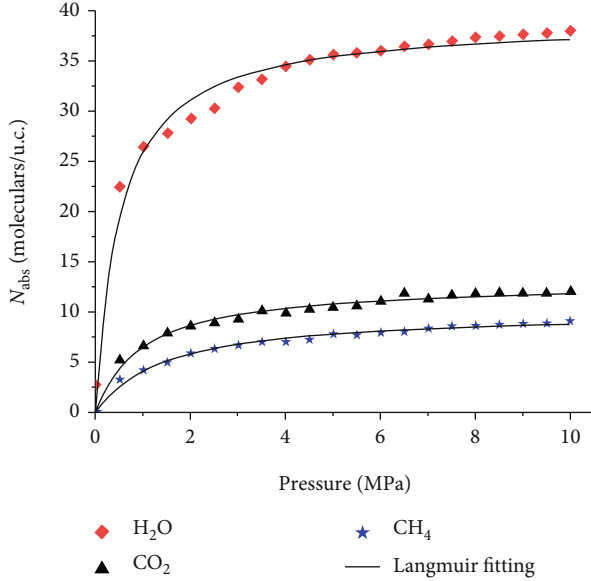


FIGURE 4: Adsorption isotherms of lignite on  $\text{CH}_4$ ,  $\text{CO}_2$ , and  $\text{H}_2\text{O}$ .

one time along the direction  $AB$  through the task term “supercell” in the Build module of MS software. The molecular configuration of  $\text{CH}_4$ ,  $\text{CO}_2$ , and  $\text{H}_2\text{O}$  in lignite molecular cells was observed from a different perspective.

The saturated molecular configurations of  $\text{CH}_4$ ,  $\text{CO}_2$ , and  $\text{H}_2\text{O}$  adsorption in lignite molecules are shown in Figure 5. Distributions of the adsorbed  $\text{CH}_4$ ,  $\text{CO}_2$ , and  $\text{H}_2\text{O}$  molecules in lignite molecules can be seen clearly, and all adsorbate molecules distribute at two sides of the lignite molecular chain. Specifically,  $\text{CH}_4$  molecules are in clustering distribution and present the conformation of pairwise crossing ethane.  $\text{CO}_2$  molecules are in parallel or crossing and even vertical arrangement. For the  $\text{H}_2\text{O}$  molecules, the hydrogen atoms point to the coal molecules or oxygen atoms in surrounding  $\text{H}_2\text{O}$  molecules as a response to the hydrogen bond energy.

Under the same condition, the adsorbed quantities of  $\text{CH}_4$ ,  $\text{CO}_2$ , and  $\text{H}_2\text{O}$  in the saturated configuration of lignite vary. The adsorbed quantity of  $\text{H}_2\text{O}$  is far higher than those of  $\text{CH}_4$  and  $\text{CO}_2$ , and the adsorbed quantity of  $\text{CO}_2$  is higher than that of  $\text{CH}_4$ , indicating that  $\text{CO}_2$  adsorption is more advantageous than  $\text{CH}_4$  adsorption in lignite. With respect to the adsorbed quantity of  $\text{CH}_4$ ,  $\text{CO}_2$ , and  $\text{H}_2\text{O}$ , there is a law of  $\text{H}_2\text{O} > \text{CO}_2 > \text{CH}_4$ , which conforms to the variation law of isothermal adsorption curves gained from simulation.

For coal molecules with fixed pore diameter distributions, the MD diameters of adsorbates (0.38 nm, 0.33 nm, and 0.265 nm for  $\text{CH}_4$ ,  $\text{CO}_2$ , and  $\text{H}_2\text{O}$  molecules) determine their adsorption behaviors in coals. Only when coals with pore diameter larger than the diameter of adsorbates can the adsorbates be absorbed effectively [26]. When lignite adsorbs  $\text{CH}_4$ ,  $\text{CO}_2$ , and  $\text{H}_2\text{O}$ , it is found that molecular diameter is inversely proportional to adsorption capacity. This proves that the adsorption capacity of  $\text{H}_2\text{O}$  in lignite is higher than those of  $\text{CH}_4$  and  $\text{CO}_2$ . In fact, the interaction between lignite molecules and  $\text{H}_2\text{O}$  molecules is stronger in the

adsorption process, which is mainly caused by different interaction energies during gas molecular adsorption in lignite.

**3.3. Adsorption Energy.** During the simulation process, the energy of the unit cell system after every adding of adsorbate molecules can be recorded. This energy is the difference between energy of the adsorption composite structure and energies of adsorbents and adsorbates. The adsorption energy can be calculated according to

$$\Delta E_{\text{ads}} = E_{\text{adsorbent/adsorbate}} - E_{\text{adsorbent}} - E_{\text{adsorbate}}, \quad (11)$$

where  $\Delta E_{\text{ads}}$  is the adsorption energy of adsorbates after the occurrence of adsorption;  $E_{\text{adsorbent/adsorbate}}$  is the total energy of the whole adsorption system after the occurrence of adsorption behaviors;  $E_{\text{adsorbent}}$  is the energy of adsorbent before adsorption, that is, energy of lignite cell model; and  $E_{\text{adsorbate}}$  is the energy of adsorbates before adsorption, which refers to energies of  $\text{CH}_4$ ,  $\text{CO}_2$ , and  $\text{H}_2\text{O}$  molecular models.

Heats are released during gas molecule adsorption, thus resulting in the decreasing energy of the whole system. With the increase in the number of adsorbate molecules, the total system energy after adsorption presents a downward trend until reaching the minimum. Subsequently, no adsorption occurs by adding adsorbate molecules. Instead, there are molecular repulsions and the total system energy increases gradually. The number of adsorbate molecules when the total system energy is the lowest refers to the saturated adsorption capacity of the adsorbate.

**3.3.1. Energy Change of Adsorbed  $\text{CH}_4$  Gas Molecules.** It can be seen from Figure 6 that  $E_c$  and  $E_v$  play positive roles in the adsorption process of  $\text{CH}_4$  before saturated adsorption in lignite molecular cells. However,  $E_c$  makes a tiny contribution, and  $E_v$  takes the dominant role in the adsorption of  $\text{CH}_4$ . The total system energy reaches the lowest, and the system achieves the saturation state after the unit cell adsorbs 7  $\text{CH}_4$  molecules. Subsequently, the adsorption system begins to repel  $\text{CH}_4$  molecules after adding gas molecules.

**3.3.2. Energy Change of Adsorbed  $\text{CO}_2$  Gas Molecules.** It can be seen from Figure 7 that  $E_c$ ,  $E_v$ , and  $E_{b-H}$  play positive roles in the adsorption process of  $\text{CO}_2$  before saturated adsorption in lignite molecular cells. However,  $E_{b-H}$  makes a tiny contribution, while  $E_c$  and  $E_v$  take the dominant role in the adsorption of  $\text{CO}_2$ . The total system energy reaches the lowest and the system achieves the saturation state after the unit cell adsorbs 9  $\text{CO}_2$  molecules. Subsequently, the adsorption system begins to repel  $\text{CO}_2$  molecules after adding gas molecules.

**3.3.3. Energy Change of Adsorbed  $\text{H}_2\text{O}$  Gas Molecules.** It can be seen from Figure 8 that the changes of system energy during  $\text{H}_2\text{O}$  adsorption in lignite molecular cells are more complicated.  $E_c$  is the primary contributor to system energy, followed by  $E_{b-H}$ . The contribution of  $E_v$  is basically zero before the adsorbed quantity of  $\text{H}_2\text{O}$  molecules is lower than 12. After the adsorbed quantity of  $\text{H}_2\text{O}$  is higher than 12,  $E_v$  becomes negative energy against adsorption of  $\text{H}_2\text{O}$  molecules. Such repulsion effect increases with the increase of adsorbed quantity of  $\text{H}_2\text{O}$  molecules until reaching saturated

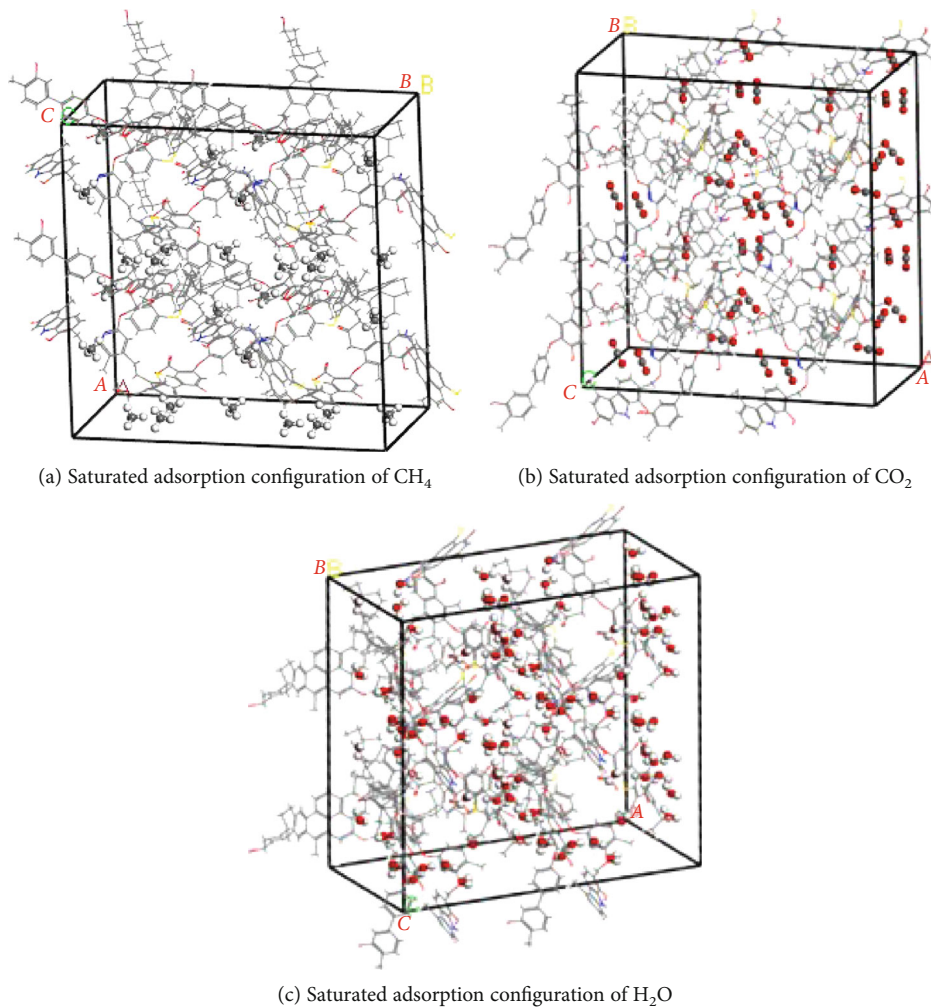


FIGURE 5: Saturated adsorption configuration of CH<sub>4</sub>, CO<sub>2</sub>, and H<sub>2</sub>O adsorbed on lignite. Color scheme: C: black; H: gray; O: red; N: blue; S: yellow.

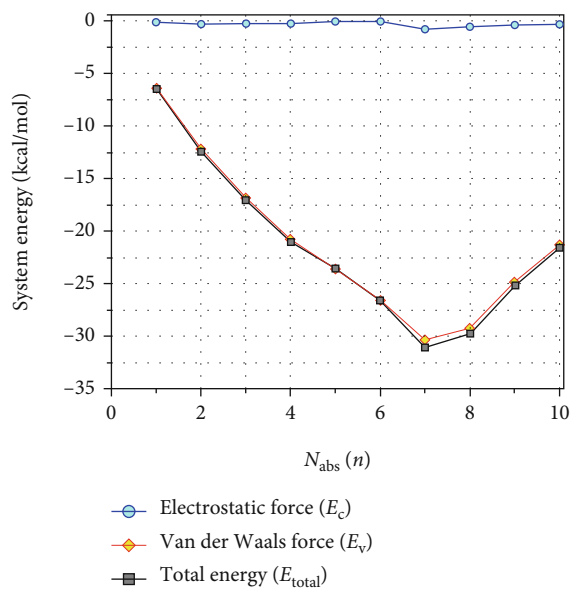


FIGURE 6: Energy changes during unit cell adsorption of different amounts of CH<sub>4</sub> molecules.

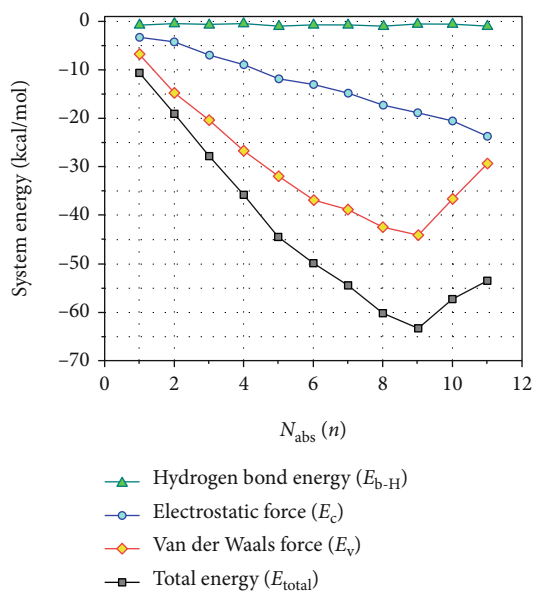


FIGURE 7: Energy changes during unit cell adsorption of different amounts of CO<sub>2</sub> molecules.

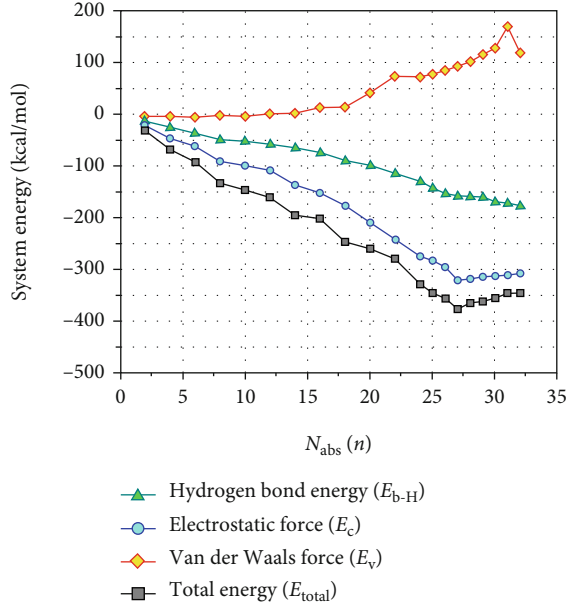


FIGURE 8: Energy changes during unit cell adsorption of different amounts of  $\text{H}_2\text{O}$  molecules.

adsorption. Although  $E_v$  hinders adsorption, the growth amplitude of the sum of  $E_c$  and  $E_{b-H}$  which are positive to the adsorption is higher than the growth amplitude of  $E_v$ , thus keeping the adsorption. The total system energy reaches the lowest, and the system achieves the saturation state after the unit cell adsorbs 27  $\text{H}_2\text{O}$  molecules. Subsequently, the adsorption system begins to repel  $\text{H}_2\text{O}$  molecules after adding gas molecules. During the repulsive interaction stage,  $E_c$  and  $E_{b-H}$  are major repulsive energies, while  $E_v$  turns to be the energy that consumes repulsion effect.

According to system energy changes during  $\text{CH}_4$ ,  $\text{CO}_2$ , and  $\text{H}_2\text{O}$  adsorption in lignite molecules, it can be seen that

- (1) system energies after  $\text{CH}_4$ ,  $\text{CO}_2$ , and  $\text{H}_2\text{O}$  adsorption in lignite molecules drop significantly. With respect to the reduction amplitudes, there is a law of  $\text{H}_2\text{O} > \text{CO}_2 > \text{CH}_4$ , indicating that  $\text{H}_2\text{O}$  adsorption capacity in coals is the highest, followed by adsorption capacities of  $\text{CO}_2$  and  $\text{CH}_4$  [14, 17, 21, 23, 26]
- (2) single lignite molecular cells reach the saturated adsorption state and the system energy is the lowest after adsorbing 7  $\text{CH}_4$  molecules, 9  $\text{CO}_2$  molecules, or 27  $\text{H}_2\text{O}$  molecules. With continuous adding of adsorbate molecules, the adsorption system begins to repel gas molecules and the total system energy increases gradually [21]
- (3) in the process of  $\text{CH}_4$ ,  $\text{CO}_2$ , and  $\text{H}_2\text{O}$  adsorption in lignite molecules, adsorption of  $\text{CH}_4$  and  $\text{CO}_2$  is typical physical adsorptions. The adsorption energy of  $\text{CH}_4$  is provided by  $E_v$  in the nonbonding energy, while the adsorption energy of  $\text{CO}_2$  is provided by  $E_c$  and  $E_v$  in the nonbonding energy together. Adsorption of  $\text{H}_2\text{O}$  involves both chemical and

physical adsorptions, and the adsorption energy of  $\text{H}_2\text{O}$  is attributed to both nonbonding energy and  $E_{b-H}$ . This conforms to previous research conclusions [23, 43–45]

**3.4. Effects of Temperature on Adsorption Behaviors.** Isothermal curves of  $\text{CH}_4$ ,  $\text{CO}_2$ , and  $\text{H}_2\text{O}$  adsorptions in lignite under 0.00–10.00 MPa and at different temperatures (283.15 K, 303.15 K, and 323.15 K) are shown in Figure 9.

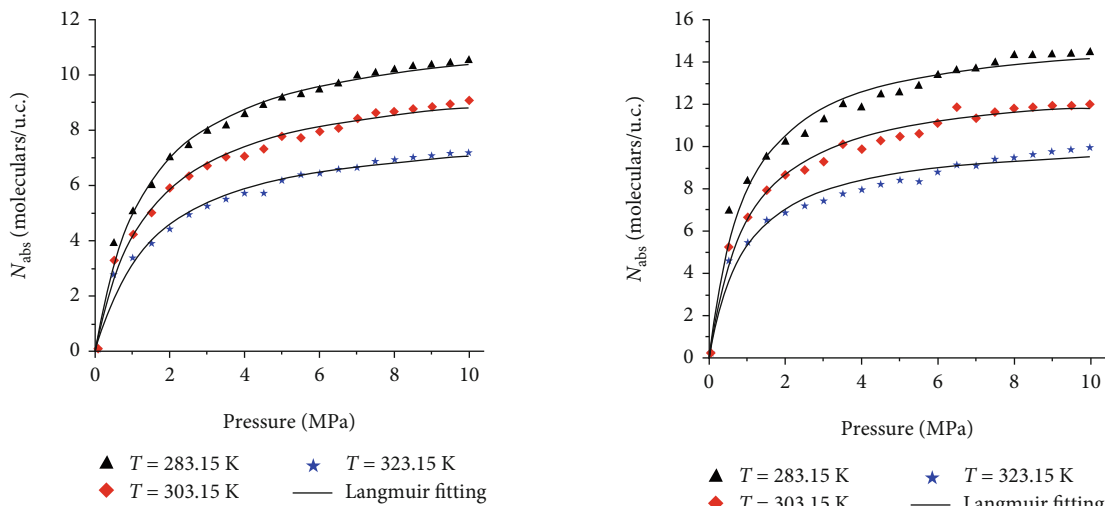
Based on single-gas adsorption in lignite molecules, it can be seen clearly that temperature can inhibit adsorption. This can be explained as follows.  $\text{CH}_4$ ,  $\text{CO}_2$ , and  $\text{H}_2\text{O}$  adsorptions in coals which are porous media belong to physical adsorption, and thermal movement of gas molecules is intensified with the increase of system temperature, thus increasing kinetic energy of adsorbate molecules. Under this circumstance, the probability for gas molecules to get rid of binding of adsorption energy increases. In particular, the probability of VDW force which promotes desorption increases, and the difficulties of capturing adsorbed gas molecules on the coal surface are increased, thus reducing adsorbing capacity [44, 46, 47]. Meanwhile, the gas molecular adsorption on the coal surface is a heat-releasing process, and temperature rise is against the heat releasing, which is the reason for decreasing adsorption capacity of lignite [48, 49].

## 4. Conclusions

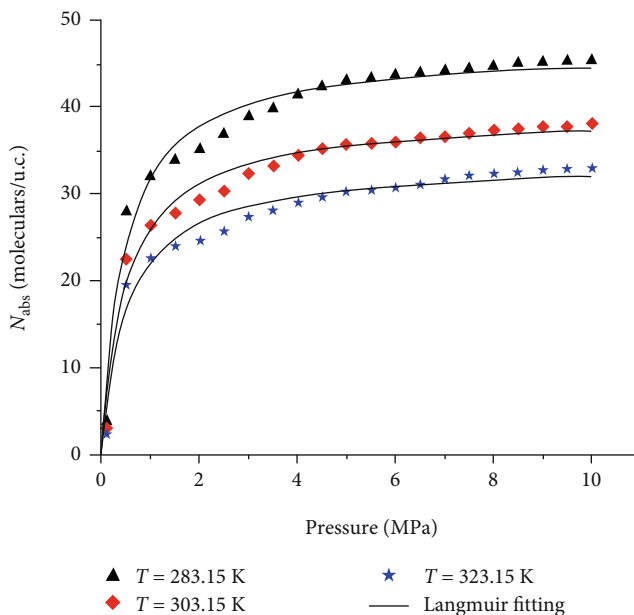
In this work, adsorption characteristics of  $\text{CH}_4$ ,  $\text{CO}_2$ , and  $\text{H}_2\text{O}$  molecules in lignite are discussed through a simulation. The selection optimization and simulation methods of the lignite molecular models are elaborated thoroughly. Moreover, adsorption capacities of  $\text{CH}_4$ ,  $\text{CO}_2$ , and  $\text{H}_2\text{O}$  in lignite molecules, saturated molecular configuration, evolutions of adsorption energies, and influences of temperature on adsorption behavior are analyzed. Some major conclusions could be drawn:

- (1) The classical Wisser model can reflect the basic features of low-metamorphism lignite comprehensively. After molecular dynamics optimization and annealing process, the lignite molecular structure becomes more compacted and has stronger stereo perception. Based on a density energy simulation, the constructed lignite molecular model is proved applicable to simulation of adsorption characteristics
- (2) Adsorption capacities of  $\text{CH}_4$ ,  $\text{CO}_2$ , and  $\text{H}_2\text{O}$  in lignite are significantly different. Given the same temperature and pressure,  $\text{H}_2\text{O}$  shows the highest ultimate adsorption capacity of these three gases in unit mass of lignite, followed by  $\text{CO}_2$  and  $\text{CH}_4$  successively. The isothermal curves present well “I-type” characteristics
- (3) A single lignite molecular cell reaches saturated adsorption upon 7  $\text{CH}_4$  molecules, 9  $\text{CO}_2$  molecules, or 27  $\text{H}_2\text{O}$  molecules. The molecular configurations of lignite molecules to  $\text{CH}_4$ ,  $\text{CO}_2$ , and  $\text{H}_2\text{O}$  gases are extracted, finding that all gas molecules distribute





(a) The lignite adsorption isotherms of CH<sub>4</sub> at different temperatures (b) The lignite adsorption isotherms of CO<sub>2</sub> at different temperatures



(c) The lignite adsorption isotherms of H<sub>2</sub>O at different temperatures

FIGURE 9: The lignite adsorption isotherms of CH<sub>4</sub>, CO<sub>2</sub>, and H<sub>2</sub>O at different temperatures.

at two sides of the lignite molecular chain. Specifically, CH<sub>4</sub> molecules are in clustering distributions and form a pairwise crossing ethane conformation. CO<sub>2</sub> molecules are in parallel or crossing and even vertical arrangement. H<sub>2</sub>O molecules point to the coal molecules or oxygen atoms in surrounding H<sub>2</sub>O molecules as a response to the hydrogen bond energies

- (4) The CH<sub>4</sub> and CO<sub>2</sub> adsorptions in lignite are typical physical adsorption, and adsorption energies are provided by nonbonding energies. However, H<sub>2</sub>O adsorption involves both physical and chemical adsorptions, with adsorption energies provided by both nonbonding energy and hydrogen bond energy

- (5) Temperature can inhibit adsorption of lignite since CH<sub>4</sub>, CO<sub>2</sub> and H<sub>2</sub>O adsorptions in lignite are physical adsorptions. With the increase of temperature, thermal movement of gas molecules is intensified. As a result, kinetic energy of adsorbate molecules increases, and the difficulties of adsorbed gas molecules are increased. Temperature rise is not in favor of the adsorption-induced heat releasing

### Data Availability

The data used to support the findings of this study are included within the article.

## Conflicts of Interest

The authors declare that they have no conflicts of interest.

## Acknowledgments

This work was supported by the National Natural Science Foundation of China (Grant No.: 51974109), the Program for Leading Talents in Scientific and Technological Innovation of Henan Province (Grant No.: 204200510032), the Scientific and Technological Projects of Henan Province (Grant No.: 202102310220), the Plan of Key Scientific Research Project of Colleges and Universities in Henan Province (Grant No.: 20A620001), the Natural Science Foundation of Henan Province of China (Grant No.: 202300410182), and the Henan Polytechnic University Doctoral Fund (Grant No.: B2019-55).

## References

- [1] J. X. Yang, Y. Q. He, and X. Y. Zhang, "Energy development trend and the coal enterprises' countermeasures in China under the background of low-carbon economy," *China Mining Magazine*, vol. 19, no. 8, pp. 58–61, 2010.
- [2] L. L. Si, H. T. Zhang, J. P. Wei, B. Li, and H. K. Han, "Modeling and experiment for effective diffusion coefficient of gas in water-saturated coal," *Fuel*, vol. 284, p. 118887, 2021.
- [3] C. Mcglade, J. Speirs, and S. Sorrell, "Unconventional gas – a review of regional and global resource estimates," *Energy*, vol. 55, pp. 571–584, 2013.
- [4] A. Stephen, A. Adebunsi, and A. Baldygin, "Bioconversion of coal: new insights from a core flooding study," *RSC Advances*, vol. 4, no. 43, pp. 22779–22791, 2014.
- [5] T. A. Moore, "Coalbed methane: a review," *International Journal of Coal Geology*, vol. 101, pp. 36–81, 2012.
- [6] Y. Xue, T. Teng, F. Dang, Z. Ma, S. Wang, and H. Xue, "Productivity analysis of fractured wells in reservoir of hydrogen and carbon based on dual-porosity medium model," *International Journal of Hydrogen Energy*, vol. 45, no. 39, pp. 20240–20249, 2020.
- [7] J. Liu, X. Liang, Y. Xue, K. Yao, and Y. Fu, "Numerical evaluation on multiphase flow and heat transfer during thermal stimulation enhanced shale gas recovery," *Applied Thermal Engineering*, vol. 178, p. 115554, 2020.
- [8] X. Liu, D. Song, X. He, Z. Wang, M. Zeng, and L. Wang, "Quantitative analysis of coal nanopore characteristics using atomic force microscopy," *Powder Technology*, vol. 346, pp. 332–340, 2019.
- [9] X. Liu, Z. Wang, D. Song, X. He, and T. Yang, "Variations in surface fractal characteristics of coal subjected to liquid CO<sub>2</sub>-phase change fracturing," *International Journal of Energy Research*, vol. 44, no. 11, pp. 8740–8753, 2020.
- [10] X. Wang and B. Lin, "How to reduce CO<sub>2</sub> emissions in China's iron and steel industry," *Renewable and Sustainable Energy Reviews*, vol. 57, pp. 1496–1505, 2016.
- [11] X. F. Xian, "The present situation of coal-bed methane mining and utilization in our country and looking forward to its industrialization," *Journal of Chongqing University*, vol. 15, no. 1, pp. 1–5, 2000.
- [12] Y. K. Ma, B. S. Nie, X. Q. He, X. C. Li, J. Q. Meng, and D. Z. Song, "Mechanism investigation on coal and gas outburst: an overview," *International Journal of Minerals, Metallurgy and Materials*, vol. 27, no. 7, pp. 872–887, 2020.
- [13] Z. Liao, X. Liu, D. Song et al., "Micro-structural damage to coal induced by liquid CO<sub>2</sub> phase change fracturing," *Natural Resources Research*, vol. 30, no. 1, pp. 1613–1627, 2021.
- [14] K. Mosher, J. J. He, Y. Y. Liu, E. Rupp, and J. Wilcox, "Molecular simulation of methane adsorption in micro- and mesoporous carbons with applications to coal and gas shale systems," *International Journal of Coal Geology*, vol. 109, pp. 36–44, 2013.
- [15] V. Prabu and N. Mallick, "Coalbed methane with CO<sub>2</sub> sequestration: an emerging clean coal technology in India," *Renewable & Sustainable Energy Reviews*, vol. 50, pp. 229–244, 2015.
- [16] M. S. A. Perera, "Influences of CO<sub>2</sub> injection into deep coal seams: a review," *Energy & Fuels*, vol. 31, no. 10, pp. 10324–10334, 2017.
- [17] W. N. Zhou, H. B. Wang, Z. Zhang, H. X. Chen, and X. L. Liu, "Molecular simulation of CO<sub>2</sub>/CH<sub>4</sub>/H<sub>2</sub>O competitive adsorption and diffusion in brown coal," *RSC Advances*, vol. 9, no. 6, pp. 3004–3011, 2019.
- [18] K. R. Matranga, A. L. Myers, and E. D. Glandt, "Storage of natural gas by adsorption on activated carbon," *Chemical Engineering Science*, vol. 47, no. 7, pp. 1569–1579, 1992.
- [19] M. R. Narkiewicz and J. P. Mathews, "Visual representation of carbon dioxide adsorption in a low-volatile bituminous coal molecular model," *Energy & Fuels*, vol. 23, no. 10, pp. 5236–5246, 2009.
- [20] S. J. Zhang, C. W. Li, and C. Ding, "Molecular fragment model of coal surface and molecular mechanics simulation of gas adsorption," *Mining Research and Development*, vol. 30, no. 1, pp. 88–91, 2010.
- [21] J. H. Xiang, F. G. Zeng, H. Z. Liang, B. Li, and X. X. Song, "Molecular simulation of the CH<sub>4</sub>/CO<sub>2</sub>/H<sub>2</sub>O adsorption onto the molecular structure of coal," *Scientia Sinica(Terrae)*, vol. 44, no. 7, pp. 1418–1428, 2014.
- [22] Y. Dang, L. M. Zhao, X. Q. Lu, J. Xu, and P. P. Sang, "Molecular simulation of CO<sub>2</sub>/CH<sub>4</sub> adsorption in brown coal: effect of oxygen-, nitrogen-, and sulfur-containing functional groups," *Applied Surface Science*, vol. 423, pp. 33–42, 2017.
- [23] Y. Song, J. Bo, and L. Wu, "Molecular simulation of CH<sub>4</sub>/CO<sub>2</sub>/H<sub>2</sub>O competitive adsorption on low rank coal vitrinite," *Physical Chemistry Chemical Physics*, vol. 19, no. 27, pp. 17773–17788, 2017.
- [24] H. Xu, W. Chu, and X. Huang, "CO<sub>2</sub> adsorption-assisted CH<sub>4</sub> desorption on carbon models of coal surface: a DFT study," *Applied Surface Science*, vol. 375, pp. 196–206, 2016.
- [25] X. F. You, M. He, W. Zhang, H. B. Wei, Q. Q. He, and L. Li, "Molecular dynamics simulations and contact angle of surfactant at the coal–water interface," *Molecular Simulation*, vol. 44, no. 9, pp. 722–727, 2018.
- [26] S. G. Li, Y. Bai, H. F. Lin, C. M. Shu, M. Yan, and L. W. Bin, "Molecular simulation of adsorption of gas in coal slit model under the action of liquid nitrogen," *Fuel*, vol. 255, p. 115775, 2019.
- [27] D. M. Gao, H. Lin, J. R. Wang, and D. Zheng, "Molecular simulation of gas adsorption characteristics and diffusion in micropores of lignite," *Fuel*, vol. 269, p. 117443, 2020.
- [28] H. X. Hu, L. Du, Y. F. Xing, and X. C. Li, "Detailed study on self- and multicomponent diffusion of CO<sub>2</sub> · CH<sub>4</sub> gas mixture in coal by molecular simulation," *Fuel*, vol. 187, pp. 220–228, 2017.

- [29] J. You, L. Tian, C. Zhang, H. X. Yao, W. Dou, and B. Fan, "Adsorption behavior of carbon dioxide and methane in bituminous coal: a molecular simulation study," *Chinese Journal of Chemical Engineering*, vol. 24, no. 9, pp. 1275–1282, 2016.
- [30] J. P. Mathews and A. L. Chaffee, "The molecular representations of coal – a review," *Fuel*, vol. 96, pp. 1–14, 2012.
- [31] P. H. Given, "The distribution of hydroxyl in coal and its relation to coal structure," *Fuel*, vol. 39, pp. 147–158, 1960.
- [32] J. H. Shinn, "Towards an understanding of the coal structure," *Fuel Processing Technology*, vol. 63, no. 8, pp. 483–497, 1984.
- [33] Y. Zhang, L. X. Zhou, and J. Zhang, "Simplified Solomon pyrolysis model and simulation of no formation in swirling coal combustion," *Journal of Chemical Industry and Engineering (China)*, vol. 54, no. 9, pp. 1274–1278, 2003.
- [34] M. L. Connolly, "Solvent-accessible surfaces of proteins and nucleic acids," *Science*, vol. 221, no. 4612, pp. 709–713, 1983.
- [35] B. Q. Dai, A. Hoadley, and L. Zhang, "Characteristics of high temperature C-CO<sub>2</sub> gasification reactivity of Victorian brown coal char and its blends with high ash fusion temperature bituminous coal," *Fuel*, vol. 202, pp. 352–365, 2017.
- [36] X. J. Li, L. Y. Cai, and H. Xu, "Feasibility study on coal seam gas flow based on molecular dynamics simulation," *Safety in Coal Mines*, vol. 39, no. 7, pp. 84–87, 2008.
- [37] Z. S. Li, Y. J. Zhao, X. N. Jia, and L. R. Zhang, "Development of molecular dynamics computer simulation," *Mechanical Management and Development*, vol. 23, no. 2, pp. 174–176, 2008.
- [38] Y. H. Wen, R. Z. Zhu, F. X. Zhou, and C. Y. Wang, *Main Techniques of Molecular Dynamics Simulation*, vol. 1, pp. 65–73, 2003.
- [39] Z. Y. Gao, S. K. Lv, J. D. Li, P. F. Yang, and C. M. Chen, "Micro-mechanism of water molecule adsorption on lignite surfaces," *Journal of Chinese Society of Power Engineering*, vol. 36, no. 4, pp. 258–264, 2016.
- [40] N. Metropolis, A. W. Rosenbluth, M. N. Rosenbluth, A. H. Teller, and E. Teller, "Equation of state calculations by fast computing machines," *Journal of Chemical Physics*, vol. 21, no. 6, pp. 1087–1092, 1953.
- [41] H. Chen, J. M. Li, and B. Sun, "Application of characteristics of the coal isothermal adsorption curve in coalbed methane research," *Journal of Chongqing University of Science and Technology*, vol. 13, no. 2, pp. 24–26, 2011.
- [42] J. F. Zhang, M. B. Clennell, K. Y. Liu, D. N. Dewhurst, M. Pervukhina, and N. Sherwood, "Molecular dynamics study of CO<sub>2</sub> sorption and transport properties in coal," *Fuel*, vol. 177, pp. 53–62, 2016.
- [43] G. C. Chen and X. F. Xian, "Ab initio study on the interaction between CH<sub>4</sub> and the coal surface," *Journal of Chongqing University*, vol. 23, no. 3, pp. 77–79, 2000.
- [44] Y. J. Cui, L. W. Zhong, and Q. Zhang, "The quantum chemical study on different rank coals surface interacting with methane," *Journal of China Coal Society*, vol. 32, no. 3, pp. 292–295, 2007.
- [45] A. A. Sizova, V. V. Sizov, and E. N. Brodskaya, "Molecular mechanisms of the effect of water on CO<sub>2</sub>/CH<sub>4</sub> mixture adsorption in slitlike carbon pores," *Colloid Journal*, vol. 80, no. 4, pp. 439–446, 2018.
- [46] T. J. Zhang, H. J. Xu, and S. G. Li, "The effect of temperature on the adsorbing capability of coal," *Journal of China Coal Society*, vol. 34, no. 6, pp. 802–805, 2009.
- [47] L. Si, J. Wei, Y. Xi et al., "The influence of long-time water intrusion on the mineral and pore structure of coal," *Fuel*, vol. 290, article 119848, 2021.
- [48] L. W. Zhong, Y. Z. Zheng, and Z. R. Yuan, "The adsorption capability of coal under integrated influence of temperature and pressure and predicted of content quantity of coal bed gas," *Journal of China Coal Society*, vol. 27, no. 6, pp. 581–585, 2002.
- [49] H. G. Sui and J. Yao, "Effect of surface chemistry for CH<sub>4</sub>/CO<sub>2</sub> adsorption in kerogen: a molecular simulation study," *Journal of Natural Gas Science and Engineering*, vol. 31, pp. 738–746, 2016.